Int. J. Electrochem. Sci., 8 **(2013)** 4583 - 4594

International Journal of
ELECTROCHEMICAL
SCIENCE
www.electrochemsci.org

Defects-controlled ZnO Nanorods with High Aspect Ratio for Ethanol Detection

Noor J. Ridha[1, 2,*], *Mohammad Hafizuddin Haji Jumali*[1,*], *Akrajas Ali Umar*[3] *and F. Alosfur*[1,2]

[1] School of Applied Physics, Faculty Science and Technology, Universiti Kebangsaan Malaysia (UKM), 43600 Bangi, Selangor, Malaysia
[2] Physics Department, College of Science, Ministry of Higher Education and Scientific Research, Baghdad, Iraq
[3] Institute of Microengineering and Nanoelectronics, Universiti Kebangsaan Malaysia, 43600 Selangor, Malaysia
[*]E-mail: nooraboalhab@yahoo.com, hafizhj@gmail.com

Received: 23 December 2012 / *Accepted:* 22 January 2013 / *Published:* 1 April 2013

A simple method to simultaneously control the aspect ratios and defects in vertically grown ZnO nanorods arrays on Si substrate was demonstrated in this work. The nanorods were grown on the substrate using seed mediated growth method by varying the number of growth solution while other parameters were kept constant. The samples were characterized by X- ray Diffraction (XRD), Energy-Dispersive X-ray (EDX), Field Emission Scanning Electron Microscope (FE-SEM) and Photoluminecence spectroscopy (PL). XRD results confirmed the presence of wurtzite ZnO structure grown strongly perpendicular to the surface of the substrate. The FE-SEM images revealed that the ZnO nanorods length increased with the number of fresh growth solutions suggesting faster growth along c axis while diameter almost unchanged. The aspect ratio of ZnO nanorod arrays exhibited strong dependency on the number of fresh solution where it was improved from 40 to 60. The possible growth mechanism of ZnO nanorods was discussed. PL emission spectrum displayed systematic reduction in broad green emission band with higher number of growth solution signifying lower defects in the nanorods. Gas sensing performance was investigated as a function of operating temperature, time and gas concentration. High sensitivity, stability and repeatability were achieved. In addition, the predicated gas sensing mechanism of ZnO nanorods was also discussed.

Keywords: zinc oxide nanorod; aspect ratio; multiple solutions.

1. INTRODUCTION

Ethanol detection nanotechnology is one of the most important technologies with huge variety of applications, which goes from the industry to the personal usage. This technology emerges as an

essential element in food industries, where gas sensors are used for controlling the fermentation process as well as in early detection of alcohol in traffic safety.

Many metal oxides have been used as an active material for ethanol sensing such as SnO_2 [1], ZnO [2] and TiO_2 [3]. The metal oxide gas sensors are mainly based on electrical conductivity variation which is highly affected by its' dimensions [4] and the presence of defects in the crystal [5]. Crystal defects may presence when small variation from stoichiometry happened during preparation [6, 7]. Therefore preparation method should be selected and conducted carefully because it greatly influences the fundamental properties and performance of the sensor.

Due to several significant advantages, vertically aligned ZnO nanorods are used as active material in high sensitivity ethanol sensor [8]. This nanostructure is relatively easy to fabricate using various techniques such as chemical vapor deposition [9], metal-organic chemical vapor deposition (MOCVD) [10, 11], pulsed laser deposition [12], self-assembly method [13] and aqueous solutions [14, 15]. There are also many efforts have been made to control the aspect ratio of ZnO nanorods such as using polymers [16], preheated solution [17, 18] and prolonged growth period [19]. However these methods are either costly, complicated, time consuming or after certain period the growth process retarded.

Multi- step growth solution was recently reported to increase the aspect ratio of ZnO nanorods [20]. In this earlier work, ammonia assisted hydrolysis technique was used to grow ZnO nanorods, where five different growth cycles were used to control the aspect ratio. The results showed both diameter and length were increased with increasing number of growth cycles. Since the length growth faster, an increment in aspect ratio was observed.

In the current work, the aspect ratio and crystal structure defects of ZnO nanorods were controlled using a seed mediated multiple growth solutions method. Unlike in the earlier report [20], the ZnO nanorods aspect ratio was increased by renewing the growth solution while the diameter unchanged which was found to be a crucial factor for gas sensitivity enhancement.

2. EXPERIMENTAL

2.1. Synthesis of ZnO nanorods

ZnO nanorods were prepared using seed mediated multiple growth solutions method, which comprised two simple steps, namely seeding and growth process. The seeding process was carried out by spin coated the glass substrate with a sol-gel solution to form a layer of ZnO nanoparticles. The sol-gel solution was prepared earlier by dissolving of 0.01 M of zinc acetate [Zn $(COOCH_3)_2 \cdot 2H_2O$] (*Sigma Aldrich)* in 5 mL ethanol. Next the coated glass substrate was heated at 100°C for 15 minutes. These procedures were repeated twice and finally an annealing process was carried out at 350°C for 1h to form a thin seed layer of ZnO nanoparticles of size ca. 15 nm.

Subsequent growth process involved immersing the annealed substrate vertically in aqueous growth solution. The growth solution was prepared using equal molar of 0.03 M zinc nitrate hydrate [Zn $(NO_3)_2 \cdot xH_2O$] and hexamethylenetetramine ($C_6H_{12}N_4$) abbreviated as HMT at 95º C. The total growth period was fixed for 6hrs. The difference among the prepared samples was the number of

growth solutions used for the growing process. The first sample (sample A) was prepared using single growth solution continuously for 6 hrs. As for the second samples (sample B) the coated substrate was immersed in the first growth solution for 3 hrs and subsequently re-immersed in a fresh growth solution for the final 3 hrs. Similar procedure was repeated for the third sample (sample C) by renewing the growth solutions two times with immersion period fixed 2 hrs for each solution. After six hrs of immersion all samples were rinsed with de-ionized water.

2.2. Characterization of ZnO nanorods

Crystal structure, phase identification and orientation of the samples were determined using X-ray diffraction (XRD) technique. The diffractometer used in this work was Bruker D8 Discover utilizing Cu-Kα radiation (λ= 1.5406 Å) with step size and scan speed of 0.025° and 1.5°/min respectively. The morphologies and structures of the ZnO nanorods samples were investigated using a field-emission scanning electron microscope (FESEM) (SUPRA 55VP) fitted with an energy-dispersive spectrometer ((EDX), Inca 400, Oxford Instruments). The optical properties of the nanorods were examined using photoluminescence (PL) spectroscopy (Edinburgh Instruments FLS920). The PL spectra were obtained using a 450 W Xenon lamp with excitation wavelength of 325 nm. All measurements were conducted at room temperature.

2.3. Gas sensing test

To investigate the ethanol sensing properties of the vertically aligned ZnO nanorods, a sensor was fabricated by a method similar to that described in earlier work [7]. A150 nm thick interdigitated silver electrode was deposited on the top of the samples as shown in Figure (1).

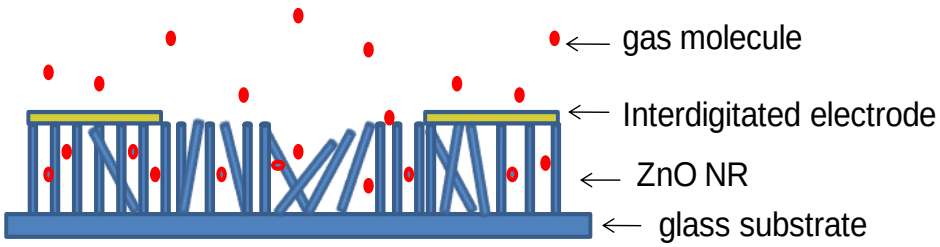

Figure 1. Schematic diagram of the interdigitated electrode on the top of the ZnO nanorods samples.

Figure 2 shows the gas sensing measurement setup used to study the ethanol sensing performance of the ZnO nanorods samples prepared in this work. The setup contains a gas providing system, a sensing chamber and a data acquisition system. The sensing mechanism is based on resistance variations of the sample resulted from exposure to different environments. To determine the changes in resistance of the sensor, a simple voltage divider circuit was used. It consists of a standard resistor (R_L) and a constant dc voltage of 5V (V_{in}) in series with the sensor. The output voltage (V_{out})

was measured across R_L. To calculate resistance of the sample in presence of air (R_a) or gas (R_g) the following equation was used:

$$R_{a\ or\ g} = \frac{(Vin - Vout)R_L}{Vout} \quad (1)$$

The sensor sensitivity (S) is defined as the ratio of the R_a to R_g,

$$S = R_a/R_g \quad (2)$$

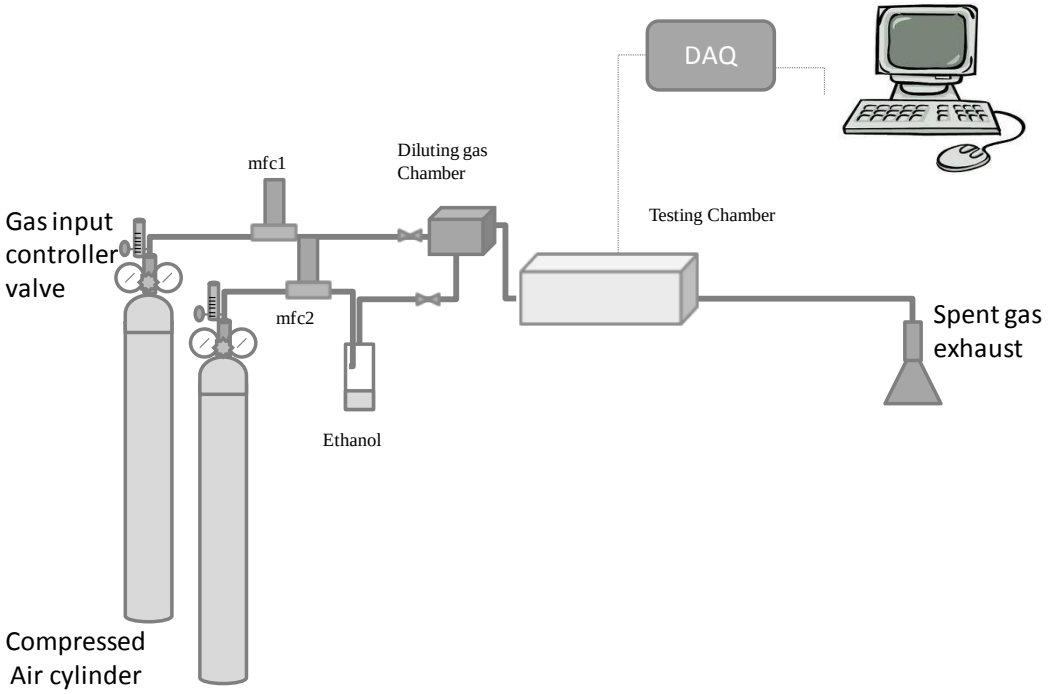

Figure 2. Schematic diagram of the experimental setup of gas sensing test.

3. RESULTS AND DISCUSSION

3.1. Structural characterizations

X ray diffractograms shown in Figure 3 confirmed the formation of pure, single phase ZnO. The crystal structure is hexagonal (wurtzite) matching with reference powder diffraction file (PDF) number 00-036-1451. The absence of amorphous hump signified that all detectable signals were purely from the samples. Generally all diffraction patterns displayed strong (002) Bragg peak indicating highly oriented ZnO growth in c-direction and retarded growth in other orientations.

The ratio of the Bragg peaks intensity between (002) and (101) determines the orientation of the ZnO growth [21]. It was found that the ratio increased as the number of growth solution increased.

Since sample C has only two prominent peaks (002) and (102) while other reflections were negligible, it exhibited the highest intensity ratio. This indicated that sample C has a well aligned 1D hexagonal structure. In addition this observation may also suggest that sample C has the highest crystalinity.

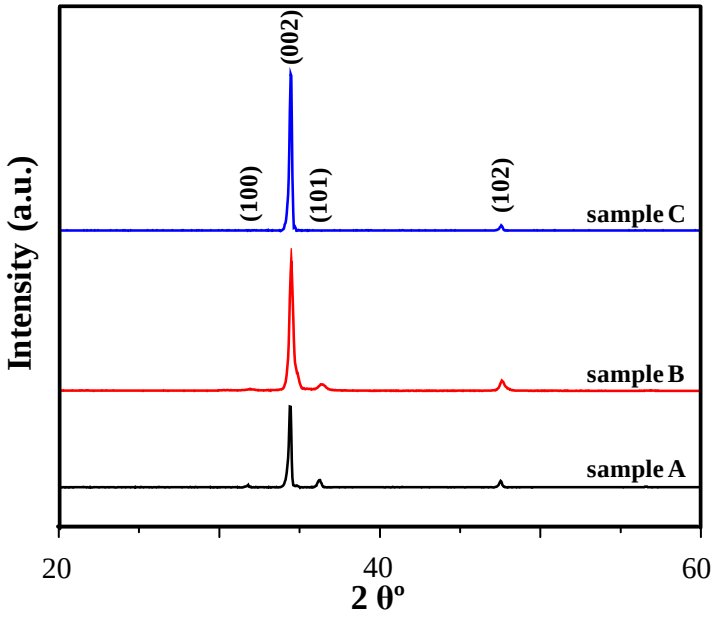

Figure 3. X ray diffractograms of ZnO nanorods for samples A, B and C.

In the present study, EDX spectra were collected to determine the purity of the samples. Figure 4 displays the EDX spectra for all samples which showed the presence of Zn, O and Si which was attributed to the substrate. No proof for the presence of other elements was detected which verified the purity of the samples. The Si peak was gradually reduced as the number of growth solutions increased which signifying an increment in the sample thickness and thus limited the electron beam penetration into Si wafer.

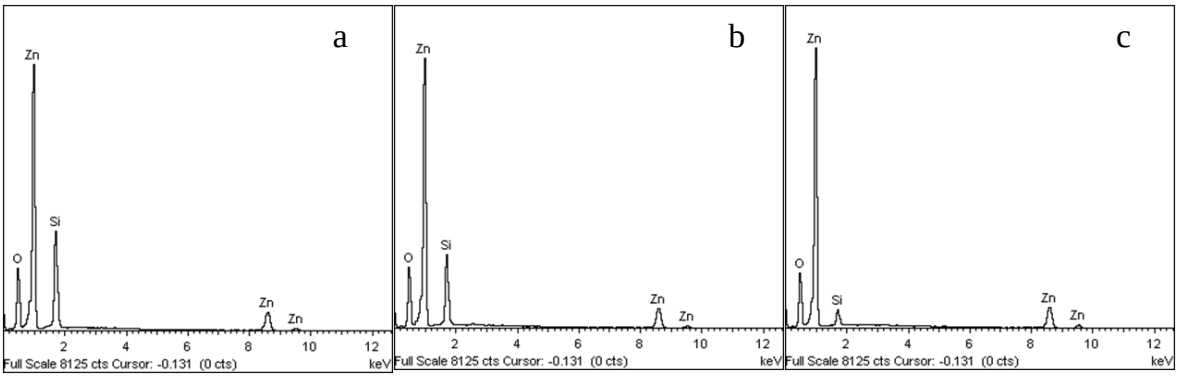

Figure 4. Energy dispersive X-ray (EDX) spectra of ZnO nanorods (a) sample A, (b) sample B and (c) sample C.

The FE-SEM micrograph shown in Figure 5 confirmed the growth of highly oriented ZnO nanorods arrays. The uniform diameter of the rods for all samples can be seen from the figure which was approximately (50 ± 5) nm. The formation of the shorter ZnO nanorods (2.00 ± 0.05) μm was achieved using a single growth solution (sample A) with average aspect ratio of 40 (Figure 5d). When the number of solution increased to two solutions (sample B), the length of the ZnO nanorods were increased to (2.50 ± 0.05) μm and average aspect ratio of 50 as shown in Figure 5e. Finally, when the number of growth solution increased to three (sample C) the average length was (3.00 ± 0.05) μm which raised the average aspect ratio to 60 Figure 5f. These results showed that the ZnO nanorods elongated by 0.5 μm when the solution numbers increased and at the same time maintained the radius. These interesting results are important and extremely useful in many fields such as solar cells and gas sensors.

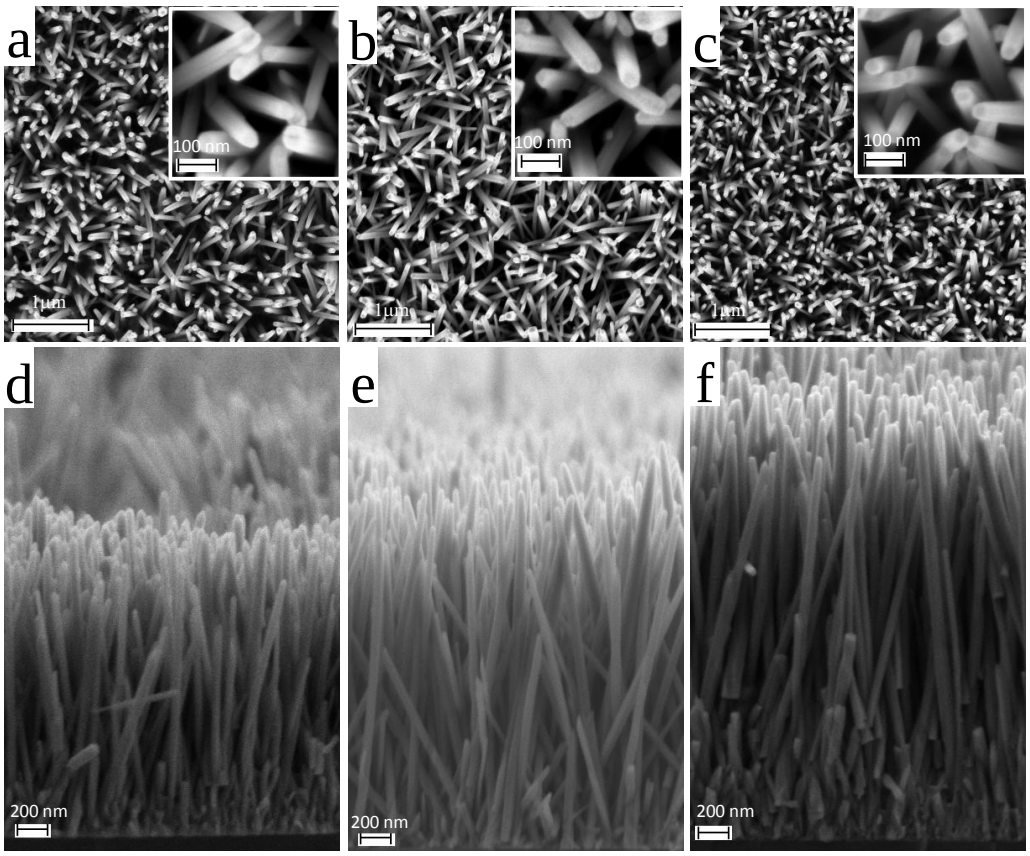

Figure 5. FE-SEM micrographs of ZnO nanorods where (a), (b) and (c) represent the top view images for samples A, B and C respectively. The lower micrographs (d), (e) and (f) represent the side view for each sample presented in the upper panel.

3.2. Growth mechanism

In general, the ZnO nanorods dimensions are strongly affected by reactant concentrations [22], type of reactant [23], type of surfactant [24, 25], growth period [26], annealing and growth temperature [27]. In addition, Baruah and Dutta [28] suggested that the diameter as well as vertical

alignment and homogeneous growth of the nanorods can be controlled by using smaller seed particle. Thus, acknowledging the importance of seed, this work gave great emphasize to produce small seeds by using low precursor concentration.

In a closed system, limited quantity of precursors was used as growth solution. Due to limited amount of OH^- and Zn $(NH_3)_4^{2+}$ ions, much faster growth of ZnO along c-axis was observed resulted from its higher surface energy [29]. The nucleation of ZnO crystals in the form of elongated nanorods continuously consumed extra Zn^{2+} ions leading to quick annihilation of the growth process. As reaction time prolonged, the growth rate decreased and finally stopped due to insufficient supplied of Zn^{2+} and OH^- ions as in sample A.

To overcome the problem of ions depletion in the growth solution, fresh growth solutions were used in order to allow the growth process to continue (as in sample B and C). Due to the polarity of ZnO nanorods, the polar exposed face (001) became electrostatically unbalanced and has high surface energy. The high surface energy can be reduced by rearrangement of the surface charge by recombination or charge transformations between surfaces. This means that the surface (001) created essentially by Zn^{+2} with c-axis orientation act as new nucleation centers attracting other molecules for further growth in c-direction rather than other direction. Nevertheless the role of HMT cannot be totally ignored [30].

3.3. The optical properties

The deep levels defects of the synthesized ZnO nanorods can be determined using the intensities ratio between ultraviolet (UV) emission (I_{UV}) and the visible (VIS) emission (I_{VIS}) obtained from the PL spectra [31]. The PL spectra for all three samples collected at room temperature were presented in Figure 6. All spectra show the identical characteristics, where two main emission bands were present. The first emission band was located in UV range at 379.5 nm which is originated from the recombination of excitons [6, 32]. In addition, there was a broad intense green emission band known as deep level emission at approximately 621 nm. This band is normally related to the structural defect in a ZnO nanomaterial resulted from oxygen vacancies [33]. Sample A showed intense visible band which signified the presence of severe structural defects in the sample. By comparison, the ZnO nanorods of samples B and C exhibited less intense green-yellow emission indicating that fewer defects were detected. Moreover the (I_{UV}/I_{VIS}) ratio of samples prepared using multiple growth solutions is significantly higher than that of sample (A) which confirmed that lower defects were induced in sample B and C.

Generally, defects in ZnO are either oxygen vacancy or formation of interstitial Zn [34]. Sufficient and constant supplies of O and Zn are crucial in order to minimize the defects. As the growth period extended in sample A, less Zn^{2+} and OH^- ions available in the solution near the active (001) surface for ZnO to grow systematically. As an attempt to reduce surface energy, the active surface randomly attracted available ions from the depleted solution resulted in formation of defects. When the growth solution renewed, it enriched the solution close to the (001) surface with Zn^{2+} and OH^- enabling a more systematic growth and thus less defects.

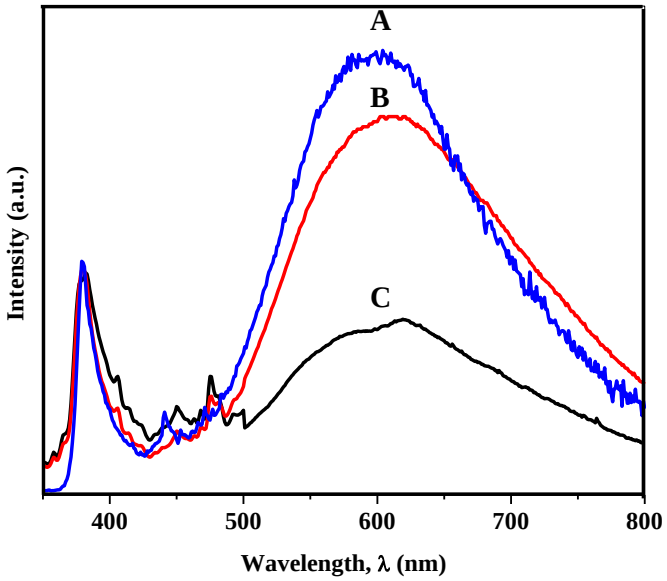

Figure 6. Photoluminous of ZnO prepared via seed mediated hydrothermal technique at 95º C for samples A, B and C.

3.4. Gas sensing performance

The gas sensing mechanism of ZnO has been described earlier [35]. In general it involves adsorption of O molecules in air by capturing electrons from the surface of ZnO. An electron depleted layers are formed on the surface of ZnO nanorods causing the carrier concentration to decrease. Consequently the resistance of ZnO nanorods in ambient air is high. When ZnO nanorods are exposed to a reducing gas such as ethanol, the density of adsorbed oxygen will be reduced. Therefore the captured electrons will return back to the depleted layer and reduces its resistance due to increasing charge carrier concentration.

In addition to well accepted factors such as morphology and surface density of the sensing materials, another important factors which influence the ZnO sensing performance are the dimension [36] and the presence of defect in the material [37]. It was reported that smaller ZnO particles exhibited better sensitivity. In addition, ZnO with high defect ratio produces more adsorption sites enabling connection with oxygen which directly raised the sensitivity.

Figure 7 shows the variation in sensitivity of ZnO nanorods prepared in this work when exposed towards ethanol at different temperatures. All samples displayed gradual increment in sensitivity and reached a maximum sensitivity at different temperatures before it decreased. It was observed that the optimum operation temperature (i.e. temperature were sensitivity is maximum) were increased as the ZnO nanorods getting longer. The sensitivity was observed to increase from 1.7 (in sample A) to around 2.3 (in sample B) before it decreased to 2.0 as shown by sample C. The highest sensitivity exhibited by sample B was believed due to synchronize effect of high aspect ratio and significantly appropriate number of defects. Although sample C appeared longer, but because of fewer defects in the nanorods, thus fewer adsorption sites were formed hence lower sensitivity was recorded.

These result indicated a delicate balance should be achieved between defects and length in order to suit the condition for high sensitivity gas sensor.

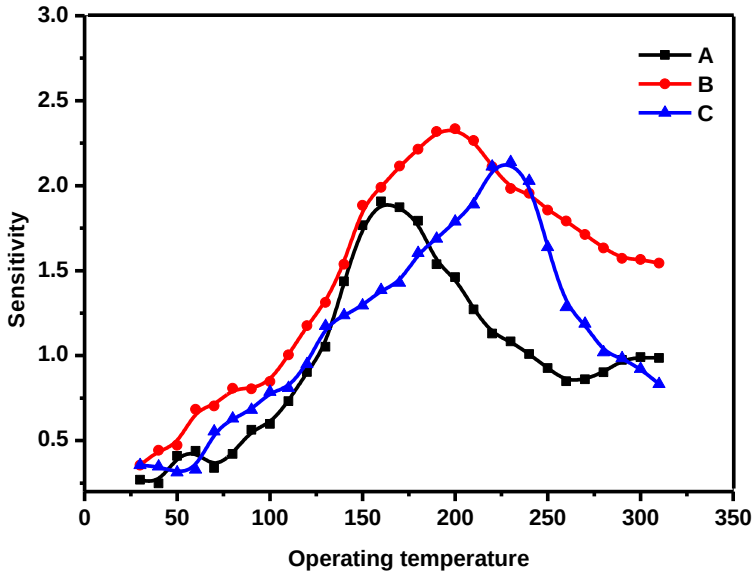

Figure 7. Optimum operating temperature, in 200 ppm ethanol vapour for samples A, B and and C.

Extensive investigations were conducted on sample B to determine the repeatability and its lowest detection limit.

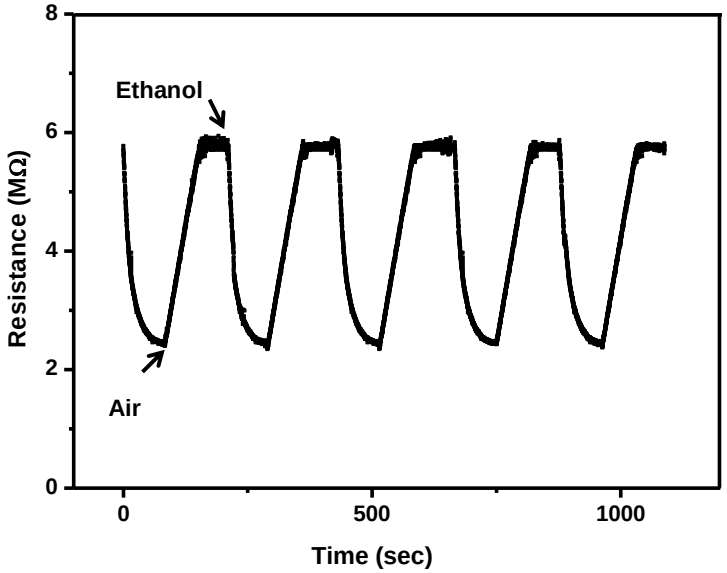

Figure 8. Repeatability of sample (B) versus time (sec) in response to 200 ppm ethanol in air at 200 ^{o}C.

Evidence of excellent repeatability characteristic of sample B as ethanol sensor observed at 200 ◦C was presented in Figure 8. In this investigation ethanol vapour with concentration of 200 ppm and dry air were alternately introduced into the chamber. The sample resistance reduced quickly in the ethanol environment until it reached saturation value. Upon the introduction of air, the resistance increased before finally reached a constant value. Important to note that sample B displayed systematic profile with constant minimum and maximum resistance throughout the test. This observation signified that this sample was extremely stable, chemically sensitive and has excellent repeatability. In addition, the response time when exposed to ethanol was 37 s while slightly longer recovery period of 61 s was recorded.

Figure 9 shows the sensitivity of sample (B) at different ethanol vapor concentrations (30 ppm up to 1000 ppm). It's obviously seen that up to 200 ppm the sensitivity increased dramatically with increasing gas concentration. Above this concentration however, no significant improvement in sensitivity was detected.

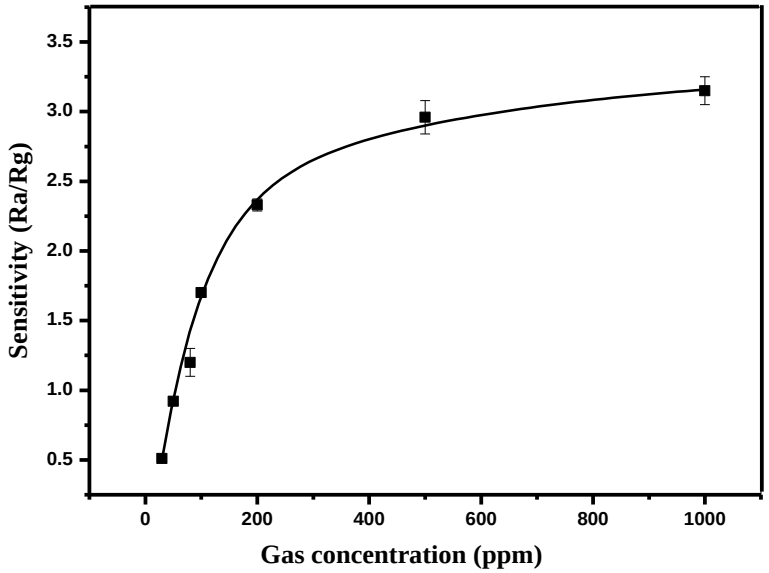

Figure 9. Sensitivity of sample (B) versus ethanol vapor concentration (ppm) at 200 ^{o}C.

4. CONCLUSION

Highly oriented crystalline ZnO nanorods arrays with different aspect ratio were successfully grown on Si substrate using seed mediated growth method. It was observed that the number of growth solution greatly influence the length and structural defects of the nanorods. The aspect ratio of nanorods was successfully increased by increasing the number of fresh growth solutions without affecting the diameter; while structural defects reduced. Ethanol detection performance was studied as a function of operating temperature, revealed that longer nanorods have higher optimum operating temperature. Sample with moderate length and defects showed high sensitivity, stability and

repeatability. These interesting results were attributed to the synchronize effects of length and defects in the nanorods.

ACKNOWLEDGEMENTS
This study was supported by Ministry of Higher Education of Malaysia under research project FRGS/1//2012/SG02/UKM/02/2). The authors are grateful to UKM for providing financial support through Zamalah program. Contribution from Mr. Mohamad Hasnul Naim for FE-SEM characterization was also appreciated.

References

1. B. Wang, L. Zhu, Y. Yang, N. Xu, and G. Yang, *J. Phys. Chem. C,* 112 (2008) 6643.
2. Y. Tak and K. Yong, *J. Phys. Chem. B,* 109 (2005) 19263.
3. X. Du, Y. Wang, Y. Mu, L. Gui, P. Wang, and Y. Tang, *Chem. Mate*r., 14 (2002) 3953.
4. E. Comini, *Anal. Chim. Acta,* 568 (2006) 28.
5. M. Wang, C. H. Ye, Y. Zhang, G. M. Hua, H. X. Wang, M. G. Kong, and L. D. Zhang, *J. Cryst. Growth,* 291 (2006) 334.
6. O. Lupan, V. Ursaki, G. Chai, L. Chow, G. Emelchenko, I. Tiginyanu, A. Gruzintsev, and A. Redkin, *Sens. Actuators, B,* 144 (2010) 56.
7. Y. F. Sun, S. B. Liu, F. L. Meng, J. Y. Liu, Z. Jin, L. T. Kong, and J. H. Liu, *Sensors,* 12 (2012) 2610.
8. J. Wang, X. Sun, Y. Yang, H. Huang, Y. Lee, O. Tan, and L. Vayssieres, *Nanotechnology,* 17 (2006) 4995.
9. J. J. Wu and S. C. Liu, *Adv. Mater.,* 14 (2002) 215.
10. E. Galoppini, J. Rochford, H. Chen, G. Saraf, Y. Lu, A. Hagfeldt, and G. Boschloo, *J. Phys. Chem. B,* 110 (2006) 16159.
11. K. S. Kim and H. W. Kim, *Physica B,* 328 (2003) 368.
12. Y. Sun, G. M. Fuge, and M. N. R. Ashfold, *Chem. Phys. Lett.,* 396 (2004) 21.
13. M. Mo, J. C. Yu, L. Zhang, and S. K. A. Li, *Adv. Mater.,* 17 (2005) 756.
14. L. Vayssieres, *Adv. Mater.,* 15 (2003) 464.
15. O. Lupan, L. Chow, G. Chai, B. Roldan, A. Naitabdi, A. Schulte, and H. Heinrich, *Mater. Sci. Eng., B,* 145 (2007) 57.
16. Y. Gao, M. Nagai, T. C. Chang, and J. J. Shyue, *Cryst. Growth Des.,* 7 (2007) 2467.
17. J. Qiu, X. Li, W. He, S. J. Park, H. K. Kim, Y. H. Hwang, J. H. Lee, and Y. D. Kim, *Nanotechnology,* 20 (2009) 155603.
18. G. Zhu, Y. Zhou, S. Wang, R. Yang, Y. Ding, X. Wang, and Y. Bando, *Nanotechnology.,* 23 (2012) 055604.
19. C. H. Ku, H. H. Yang, G. R. Chen, and J. J. Wu, *Cryst. Growth Des.,* 8 (2007) 283.
20. A. Umar, M. Rahman, R. Taslim, M. Salleh, and M. Oyama, *Int. J. Electrochem. Sci.,* 7 (2012) 8384.
21. N. Van Quy, V. A. Minh, N. Van Luan, V. N. Hung, and N. Van Hieu, *Sens. Actuators, B,* 153 (2011) 188.
22. D. Polsongkram, P. Chamninok, S. Pukird, L. Chow, O. Lupan, G. Chai, H. Khallaf, S. Park, and A. Schulte, *Physica B,* 403 (2008) 3713.
23. S. Hejazi, H. Hosseini, and M. S. Ghamsari, *J. Alloys Compd.,* 455 (2008) 353.
24. X. Sun, X. Chen, Z. Deng, and Y. Li, *Mater. Chem. Phys.,* 78 (2003) 99.
25. Z. Wang, B. Huang, X. Liu, X. Qin, X. Zhang, J. Wei, P. Wang, S. Yao, Q. Zhang, and X. Jing, *Mater. Lett.,* 62 (2008) 2637.
26. J. B. Baxter, A. M. Walker, K. V. Ommering, and E. S. Aydil, *Nanotechnology,* 17 (2006) S304.
27. S. Xu and Z. L. Wang, *Nano Res.,* 4 (2011) 1013.

28. S. Baruah and J. Dutta, *J. Sol-Gel Sci. Technol.*, 50 (2009) 456.
29. F. Solís-Pomar, E. Martínez, M. F. Meléndrez, and E. Pérez-Tijerina, *Nanoscale Res. Lett.*, 6 (2011) 1.
30. J. W. P. Hsu, Z. R. Tian, N. C. Simmons, C. M. Matzke, J. A. Voigt, and J. Liu, *Nano Lett.*, 5 (2005) 83.
31. A. Janotti and C. G. Van de Walle, *Rep. Prog. Phys.*, 72 (2009) 126501.
32. P. Yang, H. Yan, S. Mao, R. Russo, J. Johnson, R. Saykally, N. Morris, J. Pham, R. He, and H. J. Choi, *Adv. Funct. Mater.*, 12 (2002) 323.
33. M. Wang, C.-H. Ye, Y. Zhang, G.-M. Hua, H.-X. Wang, M.-G. Kong, and L.-D. Zhang, *J. Cryst. Growth*, 291 (2006) 334.
34. A. Kohan, G. Ceder, D. Morgan, and C. G. Van de Walle, *Phys. Rev. B: Condens. Matter*, 61 (2000) 15019.
35. J. Xu, J. Han, Y. Zhang, Y. Sun, and B. Xie, *Sens. Actuators, B*, 132 (2008) 334.
36. M. Arafat, B. Dinan, S. A. Akbar, and A. Haseeb, *Sensors*, 12 (2012) 7207.
37. M. W. Ahn, K. S. Park, J. H. Heo, J. G. Park, D. W. Kim, K. Choi, J. H. Lee, and S. H. Hong, *Appl. Phys. Lett.*, 93 (2008) 263103.